All-Inkjet-Printed Graphene-Gated Organic Electrochemical Transistors on Polymeric Foil as Highly-Sensitive Enzymatic Biosensors

Silvia Demuru,[*,†] *Cheng-Hua Huang,*[†] *Khaled Parvez,*[‡] *Robyn Worsley,*[‡] *Giorgio Mattana,*[§] *Benoit Piro,*[§] *Vincent Noël,*[§] *Cinzia Casiraghi,*[‡] *and Danick Briand*[*,†]

[†]School of Engineering, Ecole Polytechnique Federale de Lausanne, Neuchâtel 2000, Switzerland

[‡]Department of Chemistry, University of Manchester, Manchester M13 9PL, United Kingdom

[§]Université de Paris, ITODYS, CNRS, F-75006 Paris, France

KEYWORDS: organic electrochemical transistor, graphene, biosensor, inkjet printing, enzymatic detection, glucose

ABSTRACT. We demonstrate fully inkjet-printed graphene-gated Organic Electrochemical Transistors (OECTs) on polymeric foil for the enzymatic-based biosensing of glucose. The graphene-gated transistors exhibit better linearity, repeatability, and sensitivity than printed silver-gated devices studied in this work and other types of printed devices previously reported in the literature. Their limit of detection is 100 nM with a normalized sensitivity of 20 %/dec in the linear range of 30 to 5000 μM glucose concentrations, hence comparable with state-of-the-art OECT

devices made by lithography processes on rigid substrates and with complex multi-layer gates. Electrochemical impedance spectroscopy analysis shows that the improved sensitivity of the graphene-gated devices is related to a significant decrease of the charge-transfer resistance at the graphene electrode-electrolyte interface in the presence of glucose. The optimized sensing method and device configuration are also extended to the detection of the metabolite lactate. This study enables the development of fully-printed high-performance enzymatic OECTs with graphene sensing-gates for multi-metabolites sensing.

INTRODUCTION

Innovative electrochemical sensing configurations, electrode-bioreceptor interfaces, and functional materials are currently being studied to develop high-performance biosensors for point-of-care and continuous health monitoring.[1–6] Some of the main requirements for the next generation of biosensors include mechanical flexibility for wearable non-invasive applications,[7–9] digital manufacturing for low-cost disposable devices,[8,10] enhanced sensitivity, selectivity, short response time in the detection,[6,11] and facile miniaturization and configurability to realize integrated multi-sensing platforms.[12] Of particular interest is the possibility of non-invasive detection of metabolites in body fluids such as interstitial fluid (ISF), sweat, saliva, and tears.[5,8,13–17] Recent studies show the correlation between glucose and lactate metabolites in most of the aforementioned body fluids and blood, with some limitations for sweat glucose.[18] This is enabling the development of non-invasive glucose sensors for diabetes management,[5,17–20] or non-invasive lactate sensors for anaerobic threshold monitoring and general sport intensity.[5,21] In the case of sweat and saliva, glucose is present in the μM range (from 20's to 200's μM),[7,22] hence about 1% of the concentration found in blood plasma,[17,22] while its concentration in interstitial fluids is

similar to the one in blood.[17] Instead, the concentration of lactate is similar to the concentration observed in blood for all these biofluids and equal to 1's-10's mM.[7,17,21]

Highly selective enzymes such as glucose oxidase (GOx) and lactate oxidase (LOx) are conventionally used for the electrochemical detection of glucose and lactate, respectively,[5,22] with the possible use of artificial mediators for improving the electron transfer rate.[8,23,24] The enzymes are often immobilized on the working electrode of an amperometric three-electrode system.[5,25,26] However, the linear detection range of standard amperometric devices is generally between hundreds of μM-1 mM to several mM,[25–27] making glucose detection in some biofluids, such as sweat and saliva, difficult to be achieved. Moreover, the compact integration and fully-printing of standard amperometric cells on flexible substrates is not straightforward.[14,28,29]

Organic electrochemical transistors (OECTs)[30–33] are an interesting alternative to conventional amperometric sensors, overcoming some of their limitations. OECTs are three-terminal devices, with the source and drain electrodes connected by a conjugated polymer-polyelectrolyte channel such as the commonly used poly(3,4-ethylenedioxythiophene):polystyrene sulfonate (PEDOT:PSS). Thanks to the mixed ionic-electronic properties and the mechanical flexibility of PEDOT:PSS, OECTs allow high chemical signal amplification and better mechanical matching of the device with soft interfaces, such as the human skin, for non-invasive analysis.[34–37] Also, because digital manufacturing techniques, such as inkjet printing, can be applied for their fabrication, OECTs are promising candidates for the development of low-cost and multi-sensing biochemical platforms on flexible substrates, such as polymeric foil.[38,39]

OECT-based devices have already proved their accuracy in the detection of multiple analytes such as ions,[38,40,41] hormones,[35] proteins,[42] and metabolites.[43] With the use of a specific enzyme, only the desired metabolite will undergo a chemical reaction that leads to a shift of gate voltage,

and subsequently a change in the de-doping state of the PEDOT:PSS layer in the OECTs.[44–47] Organic electrochemical transistors for enzymatic sensing have been mostly reported for devices lithography-processed on rigid glass substrates, implementing platinum-[13,46,48] or PEDOT:PSS[24,43]-based sensing gates. These gates often include nanomaterials such as platinum nanoparticles (Pt-NPs) composites[13,48,49] and Pt/multi-wall carbon nanotubes (MWCNTs) composites[48] to enhance the sensitivity and lower the limit of detection for the enzymatic sensing of metabolites. Graphene, a single layer of graphite, is an attractive sensing material in OECTs as it has been shown to enhance the enzyme grafting process and the electrocatalytic activity towards uric acid, cholesterol, and glucose.[45] Precisely, it was used for a multi-layered gate electrode composed of enzymes/graphene oxide/polyaniline/Nafion-graphene/Pt. However, the fabrication involved sputtering of Pt, drop-cast of a Nafion-graphene aqueous solution, and then drop-cast of a polyaniline solution, hence involving a relatively complex and non-sustainable process. More recently, an OECT with source, drain, and gate electrodes made by carbon black and deposited by doctor blade has been reported,[50] but the device shows lower sensing performances compared to the state-of-the-art.

Herein, we report a completely inkjet-printed OECT device for enzymatic sensing integrating a fully-graphene gate electrode, made by printing a defect-free, highly concentrated, biocompatible, and water-based graphene ink.[51,52] The active channel and the electrical terminals of the devices are made of inkjet-printed PEDOT:PSS and silver ink, respectively. Such graphene-gated OECTs show superior sensing performance for glucose detection in an enzymatic solution, compared to the same device made by printed silver gates, and comparable performance to clean room-processed OECTs, which implemented complex nanomaterial composites on the gate electrode. Electrochemical impedance spectroscopy is used to get insights into the sensing mechanism: we

show that the response of the sensor is dominated by a strong decrease of the charge-transfer resistance at the graphene electrode-electrolyte interface in the presence of the analyte to be detected. The fully printed graphene-gated OECTs demonstrate high sensitivity and linearity for the detection of glucose and lactate in the respective physiological ranges.

EXPERIMENTAL SECTION

Functional inks. The fully-inkjet-printed organic transistors are shown in Figure 1. A silver nanoparticle-ink (Sicrys I30EG-1, PV Nano Cell) is employed for the source and drain electrical contacts, and a PEDOT:PSS ink for the conductive channel. The PEDOT:PSS ink is made by mixing a commercially available aqueous dispersion (PEDOT:PSS 1 S/cm, 1.3 wt % dispersion in H_2O, from Sigma Aldrich) with 5 vol% of dimethyl sulfoxide (DMSO, from Sigma Aldrich). The latter is added to improve the printability and the electrical conductivity of the organic layers.[53] As shown in Figure 1b, the gate electrode was either made with the graphene ink for the active area using the silver ink for its connection (graphene gate) or fully made with the silver ink for comparison (silver gate). The latter devices, made of printed silver gates, were used as reference since silver-based gates provide efficient voltage modulation[32] and silver ink is the most established conductive ink on the printed electronics market[54]. In the graphene gate configuration, the silver used for the gate electrical contact is not touching the electrolyte.

The preparation of inkjet printable graphene and its characterization (e.g. lateral size and thickness distribution of the flakes) has been previously reported.[51,52] Briefly, the graphene ink is formulated from graphite via ultrasonic-assisted liquid phase exfoliation in water using 1-pyrenesulfonic acid sodium salt (PS1). After removing the un-exfoliated graphite and excess PS1 by centrifugation, the exfoliated graphene was re-dispersed in a water-based printable solvent. The

final concentration of printable graphene ink was adjusted to ~2 mg/mL. This graphene formulation is engineered to produce defect-free, inkjet-printable, highly stable (for several months), not-cytotoxic, and concentrated graphene inks.[51]

Inkjet printing of the organic electrochemical transistors. The devices are inkjet-printed with a Dimatix DMP-2800 printer (Fujifilm) on a flexible 125 μm-thick polyimide substrate. Before printing, the silver and graphene inks are sonicated for 5 min and the PEDOT:PSS ink (with DMSO added) for 10 min. The silver and PEDOT:PSS inks are filtered with a 1 μm pore-size filter when filling the Dimatix cartridges (10-pL cartridges DMC-11610). The polyimide substrate is treated with oxygen plasma before printing. The Dimatix plate is kept at 40 ˚C during the printing. For the graphene-gated OECTs, the full fabrication steps are represented in Figure 1c and include (1) printing of ten layers of graphene ink (drop-spacing 40 μm, voltage ~20 V, jetting frequency 5 kHz, no cartridge heating), (2) sintering at 250 ˚C for 1 h, (3) printing of two layers of silver ink for the electrical contacts (drop-spacing 30 μm, voltage ~20 V, jetting frequency 5 kHz, cartridge temperature 35 ˚C), (4) sintering at 180 ˚C for 1 h, (5) printing of two layers of PEDOT:PSS ink for the channel (drop-spacing 20 μm, voltage ~20 V, jetting frequency 5 kHz, cartridge temperature 30 ˚C), and (6) curing at 120 ˚C for 20 min. All the sintering steps were performed in a ventilated oven. For the silver-gated OECTs, the fabrication steps are the same from 3 to 6, using the silver ink also for the active gate area. The design dimensions include a gate active area of about 1 x 1 mm^2 and a channel area of 1 x 3 mm^2. This design is based on a work we previously reported on OECTs with silver gates applied to multiple ions detection.[38] The gate-channel gap is about 1 mm. The graphene-gated devices have a printed graphene layer of about 1 x 2 mm^2, including a 1 mm^2 overlap with the silver contact and a 1 mm^2 active area.

The thicknesses of printed layers are measured with a Keyence VK-X1000 Series laser scanning microscope, with 50X magnification for the printed layers and 10X for the enzymatic membrane; we found an average thickness of ~50 nm for the graphene electrodes, ~1 μm for the PEDOT:PSS channels, and ~200 nm for the silver electrodes.

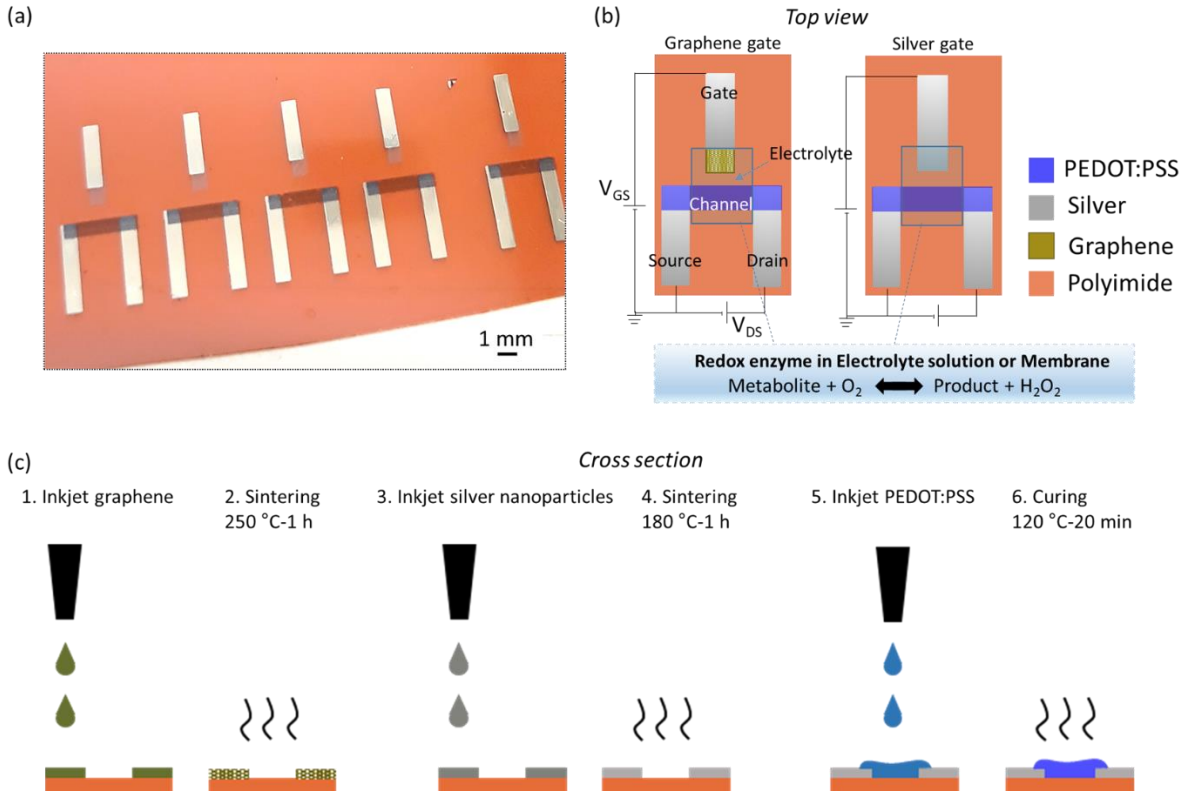

Figure 1. *Design, working principle, and fabrication of the devices. (a) Optical image of the OECTs with graphene gates, (b) top-view schematics of a graphene-gated OECT and a silver-gated OECT showing the materials and the simplified enzymatic reaction, and the bias applied during testing, and (c) cross-section with the fabrication steps.*

Enzymatic solutions. The OECTs are tested in electrolyte solutions. The enzyme is dissolved in the electrolyte solution or immobilized in a membrane around the gate electrode. Depending on the enzyme used, the targeted metabolite is converted into a different molecule defined as the product, consuming oxygen and producing hydrogen peroxide (H_2O_2), as shown in Figure 1b. For

the tests with the enzyme dissolved in solution for glucose detection, the enzymatic solution is freshly made before each experiment by carefully dissolving 10 mg of glucose oxidase (GOx) from *Aspergillus niger* (100,000-250,000 units/g, Sigma Aldrich) in 1 mL of a Phosphate Buffer Saline (PBS) solution. For lactate detection, lactate oxidase (LOx) from *Aerococcis Viridans* (100U, Sigma Aldrich) was dissolved in PBS to a concentration of 10 mg/mL and stored in aliquots before use. The PBS solution used is made of 1 mM monopotassium phosphate (KH_2PO_2, Merck), 155 mM NaCl (Sigma Aldrich), and 2.966 mM disodium phosphate (Na_2HPO_2, Merck). The ferrocene solution is made with 10 mM ferrocene (Sigma Aldrich) in ethanol as previously reported.[24]

Membrane preparation. For the tests with the immobilized GOx membrane around the gate, GOx, ferrocene, albumin from bovine serum (BSA, Sigma Aldrich), and glutaraldehyde (Sigma Aldrich) are employed. 10 mg of GOx are dissolved in 120 μL of PBS, and subsequently, 5 μL of ferrocene solution are added. The BSA solution is made by dissolving 80 mg of BSA in 1 mL of PBS, being always freshly made before the experiments. The solution of glutaraldehyde (25 %, Sigma Aldrich) is diluted to 2.5 % in DI water. Then, 50 μL of the GOx solution is mixed with 250 μL of the BSA solution, and 100 μL of glutaraldehyde 2.5 % is added to the previous mixture while carefully stirring, as described in previous methods.[55] About 3 μL of the prepared mixture was pipetted around each gate electrode of the OECTs and left for cross-linking for at least 1 hour at room temperature. The average thickness of the membrane is ~2 μm.

Sensing protocol. To confine the electrolyte solutions, a PMMA reservoir is fixed on the OECT's surface defining a gate and channel active area of 3 × 4 mm^2. Glucose and lactate stock solutions are made by dissolving glucose (D-(+)-glucose**,** Sigma Aldrich) and lactate (sodium L-

lactate, Sigma Aldrich) in PBS at different concentrations (3 μM, 1 mM, and 10 mM) and stored in the refrigerator. 30 μL of the enzymatic solution (GOx or LOx) in PBS is first added to the reservoirs, then different volumes of the glucose or lactate stock solutions are pipetted to have the sensing in time at the different concentrations. Instead, in the tests with the ferrocene mediator, 29 μL of the enzymatic solution and 1 μL of the ferrocene solution are added first to the reservoirs. The latter 29:1 ratio was chosen to have high stability during current recordings since bigger volumes of ferrocene solution caused a higher drift possibly due to ethanol evaporation. In the tests with the GOx membrane, a starting solution of 30 μL PBS, without the enzyme dissolved, is used. For the test with hydrogen peroxide, H_2O_2 (30 % w/w in H_2O, Sigma Aldrich) was diluted in PBS at different concentrations (1 mM and 10 mM). Also in the latter case, 30 μL of PBS solution is first added to the reservoirs, then different volumes of the hydrogen peroxide solutions are pipetted to have the sensing in time at the different concentrations.

Characterization and testing. The PMMA reservoirs are made by CO_2 laser (Speedy 300, Trotec) cut of 3 mm-thick PMMA plates with a double-sided silicone adhesive (ARclear 8932EE) laminated on one side. The reservoirs are attached to the sensors removing the plastic cover of the silicone adhesive. The source, drain, and gate silver contacts are insulated using a varnish to avoid possible contact with the testing solutions. The sheet resistance of the graphene electrodes is calculated from graphene resistors made with silver contact electrodes. The OECTs electrical characteristics are acquired with a semiconductor parameter analyzer (Agilent 4155A). For the sensing in time, the V_{DS} voltage is fixed to -0.4 V for both the silver and graphene-gated devices, and the V_{GS} voltage to 0.1 V for the silver and 1 V for the graphene-gated devices. The latter voltage was chosen to be close to the high-modulation region of the transistor without having water

electrolysis. Higher voltages for the silver-gated devices were causing electrode oxidation and unstable sensing behavior. The normalized sensing response is extracted as the absolute value of $\frac{I_0 - I_{glucose}}{I_0}$, with I_0 being the drain current with only the enzyme or enzyme/ferrocene in the solution, and $I_{glucose}$ the current obtained upon the addition of a given concentration of the analyte. All the signals are taken after stabilizing the I_{ds} current a few minutes after the injections of the different solutions. The Electrochemical Impedance Spectroscopy (EIS) and the cyclic voltammetry (CV) measurements are obtained using a potentiostat/galvanostat (Multi Autolab M204, Metrohm) and employing the graphene-gate or the silver-gate as the working electrodes, and a silver/silver chloride (Ag/AgCl) wire as the reference electrode. The frequency was swept from 10^5 Hz to 0.1 Hz at 10 mV of amplitude. In the case of silver, the polarization voltage chosen is equal to 0 V since higher potentials were causing noticeable oxidation. In the case of graphene, a polarization voltage close to the one applied in the transistor configuration is used (V_{dc} = 1 V). Raman measurements were performed using a Raman spectrometer (Monovista CRS+, S&I GmbH) equipped with a 514.5 nm laser with 10 mW and 100 mW laser power. The measured graphene samples were printed on a silicon substrate to reduce the background in Raman spectra. The samples measured after H_2O_2 testing were immersed for 5 minutes in a 1 mM H_2O_2 solution and then washed with DI water.

RESULTS AND DISCUSSION

Electrical characterization of the OECTs. The silver and graphene-gated OECTs electrical characteristics are analyzed in a PBS 1X solution, of similar ionic content as in biofluids. Figure 2a,c shows the output characteristics, and Figure 2b,d the transfer characteristics, for both the silver and the graphene-gated devices. The output characteristics of OECTs show a different behavior,

with optimal drain currents modulation for the silver-gated OECT, whereas a slight drain current decrease is observed for the graphene-gated ones. From the transfer characteristics, the transconductance g_m defined as $\Delta I_{DS}/\Delta V_{GS}$ can be extracted. The transconductance is of extreme relevance in OECTs targeting biosensing applications. The voltage at which the maximum peak appears is generally selected when operating in the detection mode for obtaining the maximum sensitivity.[43,56,57] The silver-gated devices show a maximum g_m of around 1 mS at 0 V while the graphene-gated devices show a continuous increase of g_m for gate voltages >0.8 V. For graphene-gated devices, g_m equals ~50 μS at 1 V. The silver-gated and Ag/AgCl-gated devices described in the literature always show a g_m peak close to 0 V for a drain-source bias around -0.4 V.[38,39] The higher voltage modulation of the graphene-gated devices is typical of carbon-based gates, as reported previously for a screen-printed carbon-gated OECT with a g_m peak at about 1.6 V for a drain-source bias of -0.4 V,[58] and a screen-printed carbon black-gate OECT with a maximum g_m at 0.7 V and a higher drain-source bias of -0.8 V.[59] Here, the extracted sheet resistance of the patterns with the graphene ink is 26 ± 4 kOhm/sq (n=10 devices), corresponding to what was previously reported for the same material,[51] and with the silver ink is 3.0 ± 0.4 Ohm/sq (n=10 devices). Considering the measured thickness of the patterns, the graphene electrodes have a resistivity of about three orders of magnitude higher than the silver ink-based electrodes. The more resistive nature of the graphene-gated devices compared to the silver-gated ones is the reason for the current modulation at much higher voltages and the difficult switching-off of the devices. Due to this, the gate voltage is fixed at 1 V for the graphene-gated devices and at 0.1 V for the silver-gated ones during the next enzymatic sensing experiments.

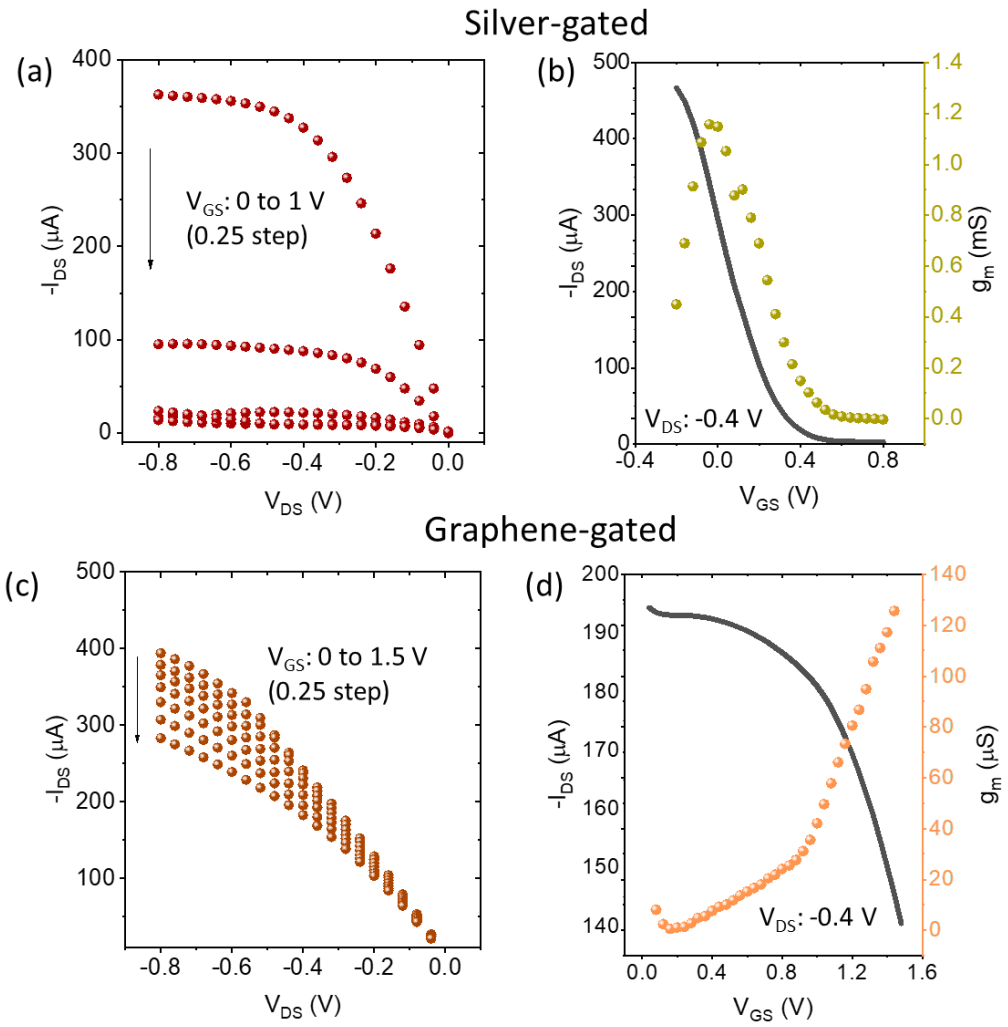

Figure 2. *Electrical characteristics. Output (a) and (b) transfer characteristics of a silver-gated OECT, and output (c) and transfer (d) of a graphene-gated OECT. Tests in PBS 1X, pH 7.*

Real-time sensing with the OECTs.

The response of the inkjet-printed OECTs is analyzed in real-time for glucose sensing. The sensing is performed in PBS solutions containing the GOx enzyme-only (Figure 3a-c) or both the enzyme and ferrocene (Figure 3d-f). Ferrocene (Fc) was added in the enzymatic solutions since it is reported to improve the detection.[22,24,43] Fc is expected to act as a mediator, competing with the

O_2/H_2O_2 redox couple.[60] The response is extracted as the absolute value of $\frac{I_0 - I_{glucose}}{I_0}$, with I_0 being the baseline current with only the enzyme or enzyme/ferrocene in the solution, and $I_{glucose}$ the current obtained upon the injection of the different concentrations of glucose. All the signals are taken after stabilization of the I_{ds} current after the injections, taking a few minutes to stabilize due to the enzymatic reaction and subsequent PEDOT:PSS dedoping.[44,56] Multiple successive injections of glucose in the linear range of ~30 to ~5000 μM are tested, the lower concentrations being in the physiological range for sweat and saliva analysis, and the higher for ISF and blood analysis in healthy subjects. Gate voltages of 0.1 V for the silver and 1 V for the graphene-gated devices are applied, relatively close to the respective transconductance peak. The latter voltage was chosen as a compromise between the g_m values and water electrolysis. The effect of the voltages applied on the gate is further analyzed using multiple electrochemical analyses in the next paragraph.

The graphene-gated devices, with and without ferrocene, show a much higher signal amplification compared to the silver-gated devices (Figure 3c,f). The calibration curves of three different devices per test condition are shown in Figure S1. The addition of ferrocene significantly improves the linearity, which increases from a normalized sensitivity value of 3.0 ± 1.8 %/dec with an extracted R^2 coefficient of 0.94 ± 0.08 without ferrocene, to a sensitivity value of 4.3 ± 2.3 %/dec with an R^2 value of 0.98 ± 0.01 for the silver-gated devices (n=3 in both cases). The same applies to the graphene-gated devices, going from sensitivity of 19.6 ± 0.7 %/dec with an R^2 coefficient of 0.91 ± 0.05 without ferrocene, to sensitivity of 18.8 ± 1.0 %/dec with an R^2 coefficient of 0.98 ± 0.02 (n=3 in both cases). Hence, ferrocene does not play a major role in terms of sensitivity, indicating that the enzymatic cycle involves the O_2 natural mediator more than Fc. Furthermore, the graphene-gated devices with ferrocene in the solution show a 4.4 times higher

sensitivity compared to the silver-gated devices also with ferrocene, combined with higher linearity and repeatability.

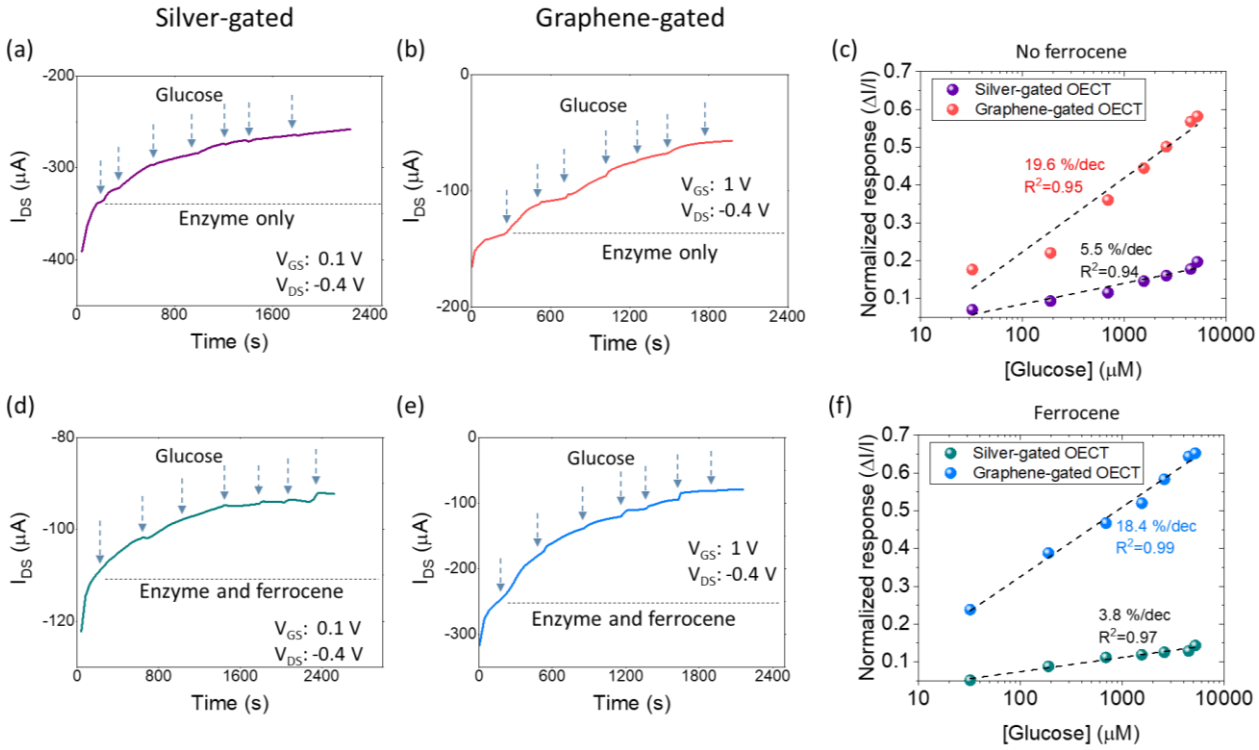

Figure 3. *Glucose sensing, using only the enzyme for the detection on a silver-gated OECT (a) and on a graphene-gated OECT (b), and corresponding calibration curves (c). Sensing using both the enzyme and ferrocene (29:1 ratio) for a silver-gated OECT (d) and a graphene-gated OECT (e), and corresponding calibration curves (f). The enzyme is dissolved in PBS 1X.*

The more stable and linear behavior in presence of ferrocene in the solution can be attributed to a decrease in the leakage current (I_{GS}), as shown in Figure S2, where the respective I_{GS} current of the devices shown in Figure 3 is presented. Both for the silver (Figure S2a,b) and graphene-gated transistors (Figure S2c,d), there is a smaller change in I_{GS} with the glucose injections in the presence of ferrocene. Also, it is noticeable that both in the presence and absence of ferrocene, the two devices have a different I_{GS} trend: the silver-gated transistors have a leakage current that goes

towards zero when increasing the glucose concentrations, possibly due to oxidation of silver causing a decrease in conductivity. On the other hand, the graphene-gated ones show an increase in current amplitude with the injections. Finally, as shown in Figure S3, actuating the graphene-gated transistors at a lower gate voltage (0.1 V, the same used for the silver-gated devices), the sensitivity is lower and more similar to the silver-gate devices. These results suggest that the higher sensitivity with graphene is also related to the fact that its electrical conductivity remains constant at higher voltages, allowing H_2O_2 oxidation and hence an increase of Faradaic current with the increase of glucose.

For the best performing devices with graphene gate and ferrocene in solution, the limit of detection was investigated using glucose concentrations in the lower range, starting from ~100 nM going up to ~1 mM (Figure S4). It can be seen that the small concentration of 100 nM glucose can be reliably detected with a signal change from the baseline of about 5 %. The presented sensing performances are compared in Table S1 with state-of-the-art on enzymatic sensing OECT devices. The graphene-gated transistors exhibit a higher sensitivity than previously reported devices with PEDOT:PSS gate electrodes using also the enzyme and ferrocene in solution,[24] platinum gate electrodes with the enzyme linked through graphene oxide,[45] and printed devices with a carbon gate electrode and enzyme in solution,[50] which exhibit similar performances as the silver-gated devices presented in this work. Our fully-printed graphene-gated OECTs are matching the sensing capabilities of those obtained with highly optimized gate electrodes, which are lithographically patterned, and require integration of hybrid nanomaterials or complex multi-layer structures.[13,43,45]

The same optimized devices with graphene and ferrocene are tested also for lactate detection with the LOx enzyme in solution (Figure S5). The sensitivity was proven at physiological ranges in biofluids (Figure S5a,b) and lower concentrations (Figure S5c,d). Lactate is found at higher

concentrations than glucose in most body fluids, hence physiological concentrations from ~2 mM to ~30 mM are used. High sensitivity equal to 21 %/dec (n=3) is also obtained for lactate sensing (Figure S5b), with a limit of detection of about 100 nM (Figure S5d) corresponding to a signal change of about 5 %, as it has been observed for glucose sensing.

As a first step towards a future implementation for point-of-care monitoring, the devices with the graphene gate are tested with an immobilized GOx membrane (Figure 4a).[55] Note that the gate electrode was not covered to not change the potential at the interface with the polymeric membrane. The real-time sensing shows a normalized sensitivity of ~10 %/dec with acceptable repeatability (n=4 devices); a LOD of ~10 µM is extracted (Figure 4b,c). The associated leakage current of the device is presented in Figure S6. The lower sensitivity and higher LOD may be explained by the number of active enzymes in the membrane. These results could be improved by optimizing the membrane formulation.

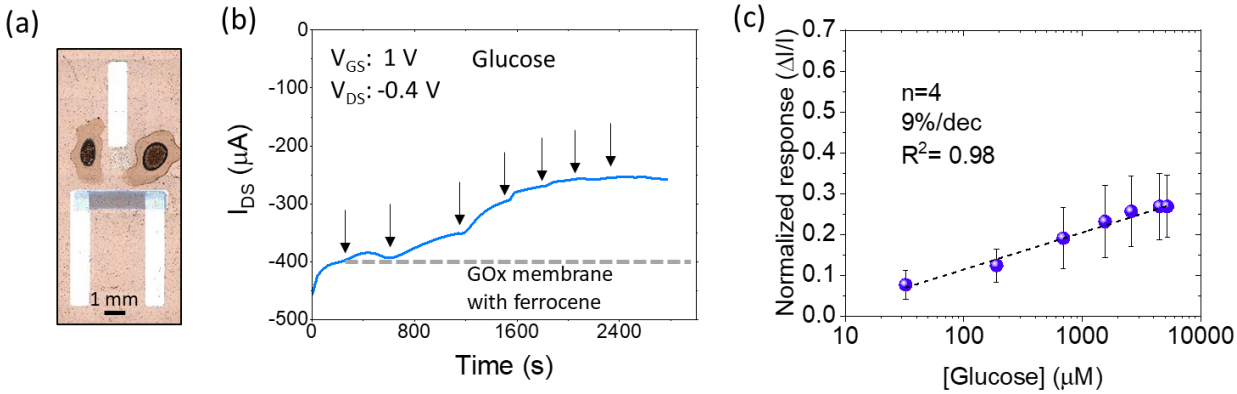

Figure 4. *Enzymatic immobilization test. (a) Optical image of the OECT with a membrane based on the GOx enzyme immobilized around the graphene-gate, (b) glucose sensing with the device, and (c) calibration curve with standard deviation for 4 devices.*

The sensing mechanism.

To better understand the sensing mechanism, the transistors are tested with only H_2O_2 in the solution (Figure S7). The different concentrations tested are the same as the previous glucose concentrations. Both the silver (Figure S7a-c) and the graphene-gated (Figure S7d-f) devices show very similar sensing responses as for the devices tested with glucose and the enzyme.

The detection mechanism is further investigated using electrochemical impedance spectroscopy (Figure 5a,b). The DC voltage applied during the impedance measurement is close to the one applied during the sensing experiment (close to the transconductance peak). The EIS measurements are performed with the same electrolyte solutions used in the OECT configuration; with only the enzyme dissolved in PBS, then adding ferrocene to the previous solution, and finally adding glucose at a fixed concentration of 700 μM. The typical Nyquist plots show that the impedance of the silver gate electrode does not significantly change in the presence of glucose (Figure 5a), with some variability among devices due possibly to occurring oxidation processes. Hence, the changes in current observed in the silver-gated OECT configuration during sensing may be due to local variations of pH due to the H^+ produced by the enzymatic reaction,[61] and subsequently de-doping the PEDOT:PSS channel.[33] On the other hand, for the printed graphene electrodes, a significant change in the charge-transfer resistance is observed from the Nyquist plots after the addition of glucose (Figure 5b). The values extracted from the fitting with the Randles circuit are reported in Table S2. While the change of charge transfer resistance (R_{ct}) before and after the addition of ferrocene is small, from 5.40 ± 0.60 MOhm to 6.60 ± 1.20 MOhm, the addition of glucose strongly decreases the R_{ct} value to 1.08 ± 0.45 MOhm (6.1 times less). Considering the double-layer capacitance (C_{dl}), it only slightly decreases with the addition of glucose, passing from about 220 nF to 200 nF. The initial high interfacial resistance of the graphene electrodes, leading

to a large potential drop at the gate-electrolyte interface, is related to the high sensitivity obtained during the enzymatic sensing.[47] In fact, the decrease of the potential drop at the electrolyte/gate interface with the enzymatic reaction leads to an increase of the potential drop at the channel/electrolyte interface and hence a higher influence of V_{GS} on I_{DS} resulting in a better modulation.

The role of ferrocene in graphene-gated devices is further investigated by cyclic voltammetry (Figure S8a). The measurement is performed with the same experimental conditions as in the previous EIS measurement. The ferrocene/ferrocenium low potential and reversible redox behavior can be seen in the CV. After the addition of glucose, no significant change of the Fc electrochemical signal is observed while an increase of current at high voltages is seen, close to the graphene-electrode polarization voltage in the OECT configuration and the EIS test (1 V); this current is probably due to H_2O_2 oxidation. In fact, a similar increase of current in the CV at high voltages can be seen in Figure S8b, where the graphene electrodes are tested with only H_2O_2 in the solution. Hence, the sensing is unlikely related to an Fc-mediated electron transfer,[43] confirming that the transduction of the enzymatic activity is based on the detection of H_2O_2. The more linear and reproducible sensing behavior with ferrocene can be explained by the fact that this redox couple can stabilize the solution potential, acting as a redox buffer.[62]

The proposed detection mechanism is that the produced H_2O_2 from the enzymatic reaction is oxidized at the sensing graphene-electrode interface, and the current produced is proportional to the glucose amount in solution (Figure 5c,d). Electrons are likely transferred from the reduced enzyme to the graphene electrode thanks to the O_2/H_2O_2 redox couple, leading to a decrease of the R_{ct} resistance at the gate, which results in the rise of the voltage at the gate-electrolyte interface (Figure 5e,f). Even if the silver-gated transistors have superior electrical characteristics, this

electrochemical reaction at the graphene-gate interface is the reason for the improved sensitivity with the graphene-gated devices. This transduction principle was previously reported for other enzymatic-based OECTs.[43,46] To analyze if a change of material composition could also play a role in the sensing process, Raman spectroscopy was performed on the graphene layers at different conditions (Figure S10). The Raman spectra show that the D and G peaks of the graphene stay constant after exposure to H_2O_2, demonstrating that the H_2O_2 produced from the enzymatic reaction does not alter the graphene layers.[52] The insignificant change observed after sintering and after H_2O_2 exposure confirms the stability of the printed graphene layers (Figure S10a,b).

Finally, the amplification effect of the OECTs is demonstrated in Figure S10, where the OECT configuration (Figure S10a) is compared to a 2-electrode amperometric system composed of the graphene electrode as a working electrode and an Ag wire as the auxiliary electrode (Figure S10b). The current values in the OECT configurations for glucose sensing are about three orders of magnitude higher compared to the 2-electrode amperometric measurement. The values in the 2-electrode mode are in the same order of magnitude as the leakage current. While the variations of normalized current in the 2-electrode mode are higher than the OECT mode as previously reported,[63] the capability of producing an amplified current signal with OECT allows a much lower limit of detection and higher sensitivities for low-concentrated molecules.

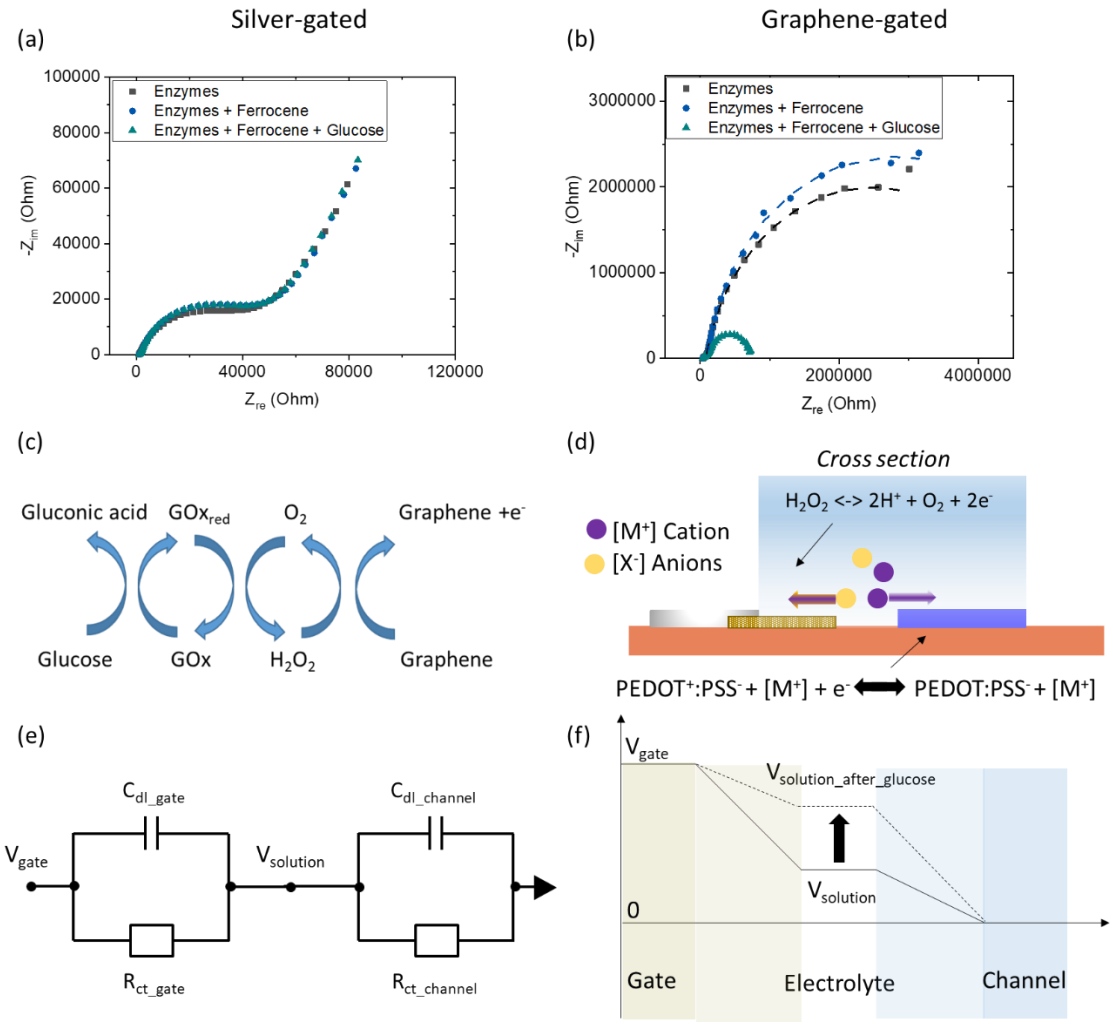

Figure 5. *Electrochemical impedance spectroscopy analysis. Nyquist plots of the silver-gate electrode (a) and the graphene-gate electrode (b) versus an Ag/AgCl reference, with only the enzyme in PBS, the enzyme and ferrocene (29:1 ratio), and adding 700 μM of glucose. (c) Enzymatic reaction with the detection at the graphene electrode interface, (d) cross-section showing the potential transduction principle of OECTs and the electrochemical reactions, (e) schematics of the extracted model with the graphene-gate electrode, and (f) the detection mechanism in terms of voltage change.*

CONCLUSIONS

This work demonstrates highly sensitive and fully-inkjet-printed enzymatic organic electrochemical transistors based on graphene gates. The printed graphene-gated OECTs show sensing performances for glucose and lactate detection in enzymatic solutions comparable to those obtained with lithography processed devices on rigid substrates and integrating complex materials as sensing gate electrodes. The OECTs with inkjet-printed graphene gates show higher sensitivity and linearity than OECTs with silver-nanoparticles gate electrodes. The repeatability of the OECT devices with graphene gates and adding ferrocene in solution is demonstrated both for glucose and lactate sensing in enzymatic solutions. The operation of the sensor with the immobilized enzyme using a membrane around the gate is demonstrated for future implementations in point-of-care analysis. Moreover, the sensing mechanism is analyzed through cyclic voltammetry and electrochemical impedance spectroscopy, and with the latter, a 6 times decrease of the charge-transfer resistance at the graphene electrode-electrolyte interface in the presence of glucose at a concentration of interest is extracted. This voltage change at the gate electrode is amplified in terms of current thanks to the modulated organic channel.

The simplicity of the fabrication process, with the optimized inkjet-printed graphene active-gate material, enables digital manufacturing of performing enzymatic OECT based sensors on polymeric foil for the realization of disposable and configurable biosensing platforms. For future applications with real biofluids, further stability and interference studies are required, including OECTs with different functionalizations in the same platform for multi-parametric analysis.

ASSOCIATED CONTENT

Supporting Information. The Supporting Information file is available free of charge.

Repeatability study, Leakage current in the OECTs during sensing, Sensing comparison, Limit of detection for glucose sensing, Lactate sensing, Leakage current with the membrane, Test with hydrogen peroxide, Cyclic voltammetry measurement, Raman spectroscopy, Amplification mechanism, Literature comparison, EIS fitting for the graphene electrodes.

AUTHOR INFORMATION

Corresponding Author

*E-mail: danick.briand@epfl.ch (D.B.).

*E-mail: silvia.demuru@epfl.ch (S.D.).

ACKNOWLEDGMENT

D.B. acknowledges the funding from SNF-SINERGIA under the project WeCare (N°CRSII5_177255) and SNF under the project 206021:164028: “Aerosol Jet Tool for Additive Manufacturing and 3D Printing for Microsystems”. C.C. and K.P. acknowledge financial support by the European Commission (ICT project WASP, grant agreement No. 825213, and the Graphene Flagship Core 3, contract No. 881603). RW acknowledges the Hewlett-Packard Company for financial support in the framework of the EPSRC Graphene NOWNANO Centre for Doctoral Training (EP/L01548X/1). This work was also sponsored by the Franco-Swiss Hubert Curien Partnership "Germaine de Staël". S.D., D.B., G. M., B. P., and V. N. are grateful to the French Ministry of Foreign Affairs (MEAE), the French Ministry of Higher Education, Research and Innovation (MESRI), and the Swiss Academy of Engineering Sciences (SATW). D.B. and S.D. wish to thank Dr. Peter van der Wal for the useful advice on electrochemical analysis, and Dr. Franz-Josef Haug for his help with the Raman spectroscopy measurements.

REFERENCES

(1) Tricoli, A.; Nasiri, N.; De, S. Wearable and Miniaturized Sensor Technologies for Personalized and Preventive Medicine. *Adv. Funct. Mater.* **2017**, *27* (1605271), 1–19. https://doi.org/10.1002/adfm.201605271.

(2) Ting, S.; Tan, M.; Giovannitti, A.; Melianas, A.; Moser, M.; Cotts, B. L.; Singh, D.; Mcculloch, I.; Salleo, A. High-Gain Chemically Gated Organic Electrochemical Transistor. *Adv. Funct. Mater.* **2021**, No. 2010868, 1–9. https://doi.org/10.1002/adfm.202010868.

(3) Mariani, F.; Gualandi, I.; Tessarolo, M.; Fraboni, B.; Scavetta, E. PEDOT: Dye-Based, Flexible Organic Electrochemical Transistor for Highly Sensitive PH Monitoring. *ACS Appl. Mater. Interfaces* **2018**, *10* (26), 22474–22484. https://doi.org/10.1021/acsami.8b04970.

(4) Pappa, A. M.; Parlak, O.; Scheiblin, G.; Mailley, P.; Salleo, A.; Owens, R. M. Organic Electronics for Point-of-Care Metabolite Monitoring. *Trends Biotechnol.* **2018**, *36* (1), 45–59. https://doi.org/10.1016/j.tibtech.2017.10.022.

(5) Sempionatto, J. R.; Lin, M.; Yin, L.; De la paz, E.; Pei, K.; Sonsa-ard, T.; de Loyola Silva, A. N.; Khorshed, A. A.; Zhang, F.; Tostado, N.; Xu, S.; Wang, J. An Epidermal Patch for the Simultaneous Monitoring of Haemodynamic and Metabolic Biomarkers. *Nat. Biomed. Eng.* **2021**, 1–12. https://doi.org/10.1038/s41551-021-00685-1.

(6) Sabaté del Río, J.; Henry, O. Y. F.; Jolly, P.; Ingber, D. E. An Antifouling Coating That Enables Affinity-Based Electrochemical Biosensing in Complex Biological Fluids. *Nat. Nanotechnol.* **2019**, *14* (12), 1143–1149. https://doi.org/10.1038/s41565-019-0566-z.

(7) Bariya, M.; Nyein, H. Y. Y.; Javey, A. Wearable Sweat Sensors. *Nat. Electron.* **2018**, *1*, 160–171. https://doi.org/10.1038/s41928-018-0043-y.

(8) Imani, S.; Bandodkar, A. J.; Mohan, A. M. V.; Kumar, R.; Yu, S.; Wang, J.; Mercier, P. P. A Wearable Chemical-Electrophysiological Hybrid Biosensing System for Real-Time Health and Fitness Monitoring. *Nat. Commun.* **2016**, *7* (11650), 1–7. https://doi.org/10.1038/ncomms11650.

(9) Paul, B.; Demuru, S.; Lafaye, C.; Saubade, M.; Briand, D. Printed Iontophoretic-Integrated Wearable Microfluidic Sweat-Sensing Patch for On-Demand Point-Of-Care Sweat Analysis. **2021**, *2000910*, 1–11. https://doi.org/10.1002/admt.202000910.

(10) Parate, K.; Rangnekar, S. V.; Jing, D.; Mendivelso-Perez, D. L.; Ding, S.; Secor, E. B.; Smith, E. A.; Hostetter, J. M.; Hersam, M. C.; Claussen, J. C. Aerosol-Jet-Printed Graphene Immunosensor for Label-Free Cytokine Monitoring in Serum. *ACS Appl. Mater. Interfaces* **2020**, *12* (7), 8592–8603. https://doi.org/10.1021/acsami.9b22183.

(11) Picca, R. A.; Manoli, K.; Macchia, E.; Sarcina, L.; Di Franco, C.; Cioffi, N.; Blasi, D.; Österbacka, R.; Torricelli, F.; Scamarcio, G.; Torsi, L. Ultimately Sensitive Organic Bioelectronic Transistor Sensors by Materials and Device Structures' Design. *Adv. Funct. Mater.* **2019**, *30* (1904513), 1–23. https://doi.org/10.1002/adfm.201904513.

(12) Gao, W.; Emaminejad, S.; Nyein, H. Y. Y.; Challa, S.; Chen, K.; Peck, A.; Fahad, H. M.; Ota, H.; Shiraki, H.; Kiriya, D.; Lien, D. H.; Brooks, G. A.; Davis, R. W.; Javey, A. Fully Integrated Wearable Sensor Arrays for Multiplexed in Situ Perspiration Analysis. *Nature* **2016**, *529* (7587), 509–514. https://doi.org/10.1038/nature16521.

(13) Ji, X.; Lau, H. Y.; Ren, X.; Peng, B.; Zhai, P.; Feng, S. P.; Chan, P. K. L. Highly Sensitive Metabolite Biosensor Based on Organic Electrochemical Transistor Integrated with Microfluidic Channel and Poly(N-Vinyl-2-Pyrrolidone)-Capped Platinum Nanoparticles. *Adv. Mater. Technol.* **2016**, *1* (5), 1–8. https://doi.org/10.1002/admt.201600042.

(14) Liu, Q.; Liu, Y.; Wu, F.; Cao, X.; Li, Z.; Alharbi, M.; Abbas, A. N.; Amer, M. R.; Zhou, C. Highly Sensitive and Wearable In2O3Nanoribbon Transistor Biosensors with Integrated On-Chip Gate for Glucose Monitoring in Body Fluids. *ACS Nano* **2018**, *12*, 1170−1178. https://doi.org/10.1021/acsnano.7b06823.

(15) Bandodkar, A. J.; Wang, J. Non-Invasive Wearable Electrochemical Sensors: A Review. *Trends Biotechnol.* **2014**, *32* (7), 363–371. https://doi.org/10.1016/j.tibtech.2014.04.005.

(16) Hong, Y. J.; Lee, H.; Kim, J.; Lee, M.; Choi, H. J.; Hyeon, T.; Kim, D. H. Multifunctional Wearable System That Integrates Sweat-Based Sensing and Vital-Sign Monitoring to

Estimate Pre-/Post-Exercise Glucose Levels. *Adv. Funct. Mater.* **2018**, *28* (47), 1–12. https://doi.org/10.1002/adfm.201805754.

(17) Heikenfeld, J.; Jajack, A.; Feldman, B.; Granger, S. W.; Gaitonde, S.; Begtrup, G.; Katchman, B. A. Accessing Analytes in Biofluids for Peripheral Biochemical Monitoring. *Nat. Biotechnol.* **2019**, *37* (4), 407–419. https://doi.org/10.1038/s41587-019-0040-3.

(18) Nyein, H. Y. Y.; Bariya, M.; Kivimäki, L.; Uusitalo, S.; Liaw, T. S.; Jansson, E.; Ahn, C. H.; Hangasky, J. A.; Zhao, J.; Lin, Y.; Happonen, T.; Chao, M.; Liedert, C.; Zhao, Y.; Tai, L. C.; Hiltunen, J.; Javey, A. Regional and Correlative Sweat Analysis Using High-Throughput Microfluidic Sensing Patches toward Decoding Sweat. *Sci. Adv.* **2019**, *5* (8), 1–12. https://doi.org/10.1126/sciadv.aaw9906.

(19) Lee, H.; Choi, T. K.; Lee, Y. B.; Cho, H. R.; Ghaffari, R.; Wang, L.; Choi, H. J.; Chung, T. D.; Lu, N.; Hyeon, T.; Choi, S. H.; Kim, D. H. A Graphene-Based Electrochemical Device with Thermoresponsive Microneedles for Diabetes Monitoring and Therapy. *Nat. Nanotechnol.* **2016**, *11*, 566–572. https://doi.org/10.1038/nnano.2016.38.

(20) Sempionatto, J. R.; Moon, J.-M.; Wang, J. Touch-Based Fingertip Blood-Free Reliable Glucose Monitoring: Personalized Data Processing for Predicting Blood Glucose Concentrations. *ACS Sensors* **2021**. https://doi.org/10.1021/acssensors.1c00139.

(21) Seki, Y.; Nakashima, D.; Shiraishi, Y.; Ryuzaki, T.; Ikura, H.; Miura, K.; Suzuki, M.; Watanabe, T.; Nagura, T.; Matsumato, M.; Nakamura, M.; Sato, K.; Fukuda, K.; Katsumata, Y. A Novel Device for Detecting Anaerobic Threshold Using Sweat Lactate during Exercise. *Sci. Rep.* **2021**, *11* (1), 1–11. https://doi.org/10.1038/s41598-021-84381-9.

(22) Nery, E. W.; Kundys, M.; Jeleń, P. S.; Jönsson-Niedziólka, M. Electrochemical Glucose Sensing: Is There Still Room for Improvement? *Anal. Chem.* **2016**, *88* (23), 11271–11282. https://doi.org/10.1021/acs.analchem.6b03151.

(23) Cass, A. E. G.; Davis, G.; Francis, G. D.; Allen, H.; Hill, O.; Aston, W. J.; Higgins, I. J.; Plotkin, E. V.; Scott, L. D. L.; Turner, A. P. F. Ferrocene-Mediated Enzyme Electrode for Amperometric Determination of Glucose. *Anal. Chem.* **1984**, *56* (4), 667–671.

https://doi.org/10.1021/ac00268a018.

(24) Shim, N. Y.; Bernards, D. A.; Macaya, D. J.; DeFranco, J. A.; Nikolou, M.; Owens, R. M.; Malliaras, G. G. All-Plastic Electrochemical Transistor for Glucose Sensing Using a Ferrocene Mediator. *Sensors* **2009**, *9* (12), 9896–9902. https://doi.org/10.3390/s91209896.

(25) Xuan, X.; Yoon, H. S.; Park, J. Y. A Wearable Electrochemical Glucose Sensor Based on Simple and Low-Cost Fabrication Supported Micro-Patterned Reduced Graphene Oxide Nanocomposite Electrode on Flexible Substrate. *Biosens. Bioelectron.* **2018**, *109*, 75–82. https://doi.org/10.1016/j.bios.2018.02.054.

(26) Jia, W.; Bandodkar, A. J.; Valdés-Ramírez, G.; Windmiller, J. R.; Yang, Z.; Ramírez, J.; Chan, G.; Wang, J. Electrochemical Tattoo Biosensors for Real-Time Noninvasive Lactate Monitoring in Human Perspiration. *Anal. Chem.* **2013**, *85*, 6553−6560. https://doi.org/10.1021/ac401573r.

(27) Demuru, S.; Haque, R.; Joho, M. O.; Bionaz, A.; Van Der Wal, P.; Briand, D. 3D-Integration of Printed Electrochemical Sensors in Pet Microfluidics for Biochemical Sensing. *2019 20th Int. Conf. Solid-State Sensors, Actuators Microsystems Eurosensors XXXIII, TRANSDUCERS 2019 EUROSENSORS XXXIII* **2019**, No. August, 2464–2467. https://doi.org/10.1109/TRANSDUCERS.2019.8808497.

(28) Scheiblin, G.; Coppard, R.; Owens, R. M.; Mailley, P.; Malliaras, G. G. Referenceless PH Sensor Using Organic Electrochemical Transistors. *Adv. Mater. Technol.* **2017**, *2* (1600141), 1–5. https://doi.org/10.1002/admt.201600141.

(29) Guinovart, T.; Crespo, G. A.; Rius, F. X.; Andrade, F. J. A Reference Electrode Based on Polyvinyl Butyral (PVB) Polymer for Decentralized Chemical Measurements. *Anal. Chim. Acta* **2014**, *821*, 72–80. https://doi.org/10.1016/j.aca.2014.02.028.

(30) Khodagholy, D.; Rivnay, J.; Sessolo, M.; Gurfinkel, M.; Leleux, P.; Jimison, L. H.; Stavrinidou, E.; Herve, T.; Sanaur, S.; Owens, R. M.; Malliaras, G. G. High Transconductance Organic Electrochemical Transistors. *Nat. Commun.* **2013**, *4*, 1–6. https://doi.org/10.1038/ncomms3133.

(31) Rivnay, J.; Inal, S.; Salleo, A.; Berggren, M.; Malliaras, G. G. Organic Electrochemical Transistors. *Nat. Rev. Mater.* **2018**, *3* (17086), 1–13. https://doi.org/10.1038/natrevmats.2017.86.

(32) Ghittorelli, M.; Lingstedt, L.; Romele, P.; Cra, N. I.; Kovács-vajna, Z. M.; Blom, P. W. M.; Torricelli, F. High-Sensitivity Ion Detection at Low Voltages with Current-Driven Organic Electrochemical Transistors. *Nat. Commun.* **2018**, *9* (1441), 1–10. https://doi.org/10.1038/s41467-018-03932-3.

(33) Lin, P.; Yan, F.; Chan, H. L. W. Ion-Sensitive Properties of Organic Electrochemical Transistors. *ACS Appl. Mater. Interfaces* **2010**, *2* (6), 1637–1641. https://doi.org/10.1021/am100154e.

(34) Rivnay, J.; Leleux, P.; Ferro, M.; Sessolo, M.; Williamson, A.; Koutsouras, D. A.; Khodagholy, D.; Ramuz, M.; Strakosas, X.; Owens, R. M.; Benar, C.; Badier, J. M.; Bernard, C.; Malliaras, G. G. High-Performance Transistors for Bioelectronics through Tuning of Channel Thickness. *Sci. Adv.* **2015**, *1* (4), 1–6. https://doi.org/10.1126/sciadv.1400251.

(35) Parlak, O.; Keene, S. T.; Marais, A.; Curto, V. F.; Salleo, A. Molecularly Selective Nanoporous Membrane-Based Wearable Organic Electrochemical Device for Noninvasive Cortisol Sensing. *Sci. Adv.* **2018**, *4* (7), 1–10. https://doi.org/10.1126/sciadv.aar2904.

(36) Tybrandt, K.; Zozoulenko, I. V; Berggren, M. Chemical Potential – Electric Double Layer Coupling in Conjugated Polymer – Polyelectrolyte Blends. *Sci. Adv.* **2018**, *3*, 1–7.

(37) Kaphle, V.; Paudel, P. R.; Dahal, D.; Radha Krishnan, R. K.; Lüssem, B. Finding the Equilibrium of Organic Electrochemical Transistors. *Nat. Commun.* **2020**, *11* (2515), 1–11. https://doi.org/10.1038/s41467-020-16252-2.

(38) Demuru, S.; Kunnel, B. P.; Briand, D. Real-Time Multi-Ion Detection in the Sweat Concentration Range Enabled by Flexible, Printed, and Microfluidics-Integrated Organic Transistor Arrays. *Adv. Mater. Technol.* **2020**, *2000328*, 1–9. https://doi.org/10.1002/admt.202000328.

(39) Romele, P.; Ghittorelli, M.; Kovács-Vajna, Z. M.; Torricelli, F. Ion Buffering and Interface Charge Enable High Performance Electronics with Organic Electrochemical Transistors. *Nat. Commun.* **2019**, *10* (1), 1–11. https://doi.org/10.1038/s41467-019-11073-4.

(40) Pierre, A.; Doris, S. E.; Lujan, R.; Street, R. A. Monolithic Integration of Ion-Selective Organic Electrochemical Transistors with Thin Film Transistors on Flexible Substrates. *Adv. Mater. Technol.* **2019**, *4* (1800577), 1–5. https://doi.org/10.1002/admt.201800577.

(41) Demuru, S.; Kunnel, B. P.; Briand, D. Biosensors and Bioelectronics : X Thin Film Organic Electrochemical Transistors Based on Hybrid PANI / PEDOT : PSS Active Layers for Enhanced PH Sensing. *Biosens. Bioelectron. X* **2021**, *7* (100065), 1–9. https://doi.org/10.1016/j.biosx.2021.100065.

(42) Gentili, D.; D'Angelo, P.; Militano, F.; Mazzei, R.; Poerio, T.; Brucale, M.; Tarabella, G.; Bonetti, S.; Marasso, S. L.; Cocuzza, M.; Giorno, L.; Iannotta, S.; Cavallini, M. Integration of Organic Electrochemical Transistors and Immuno-Affinity Membranes for Label-Free Detection of Interleukin-6 in the Physiological Concentration Range through Antibody-Antigen Recognition. *J. Mater. Chem. B* **2018**, *6* (33), 5400–5406. https://doi.org/10.1039/c8tb01697f.

(43) Pappa, A. M.; Curto, V. F.; Braendlein, M.; Strakosas, X.; Donahue, M. J.; Fiocchi, M.; Malliaras, G. G.; Owens, R. M. Organic Transistor Arrays Integrated with Finger-Powered Microfluidics for Multianalyte Saliva Testing. *Adv. Healthc. Mater.* **2016**, *5* (17), 2295–2302. https://doi.org/10.1002/adhm.201600494.

(44) Yang, S. Y.; Cicoira, F.; Byrne, R.; Benito-Lopez, F.; Diamond, D.; Owens, R. M.; Malliaras, G. G. Electrochemical Transistors with Ionic Liquids for Enzymatic Sensing. *Chem. Commun.* **2010**, *46* (42), 7972–7974. https://doi.org/10.1039/c0cc02064h.

(45) Liao, C.; Mak, C.; Zhang, M.; Chan, H. L. W.; Yan, F. Flexible Organic Electrochemical Transistors for Highly Selective Enzyme Biosensors and Used for Saliva Testing. *Adv. Mater.* **2015**, *27* (4), 676–681. https://doi.org/10.1002/adma.201404378.

(46) Bernards, D. A.; Macaya, D. J.; Nikolou, M.; Defranco, J. A.; Takamatsu, S.; Malliaras, G.

G. Enzymatic Sensing with Organic Electrochemical Transistors. *J. Mater. Chem.* **2008**, *18*, 116–120. https://doi.org/10.1039/b713122d.

(47) Kergoat, L.; Piro, B.; Berggren, M.; Horowitz, G.; Pham, M. C. Advances in Organic Transistor-Based Biosensors: From Organic Electrochemical Transistors to Electrolyte-Gated Organic Field-Effect Transistors. *Analytical and Bioanalytical Chemistry*. 2012, pp 1813–1826. https://doi.org/10.1007/s00216-011-5363-y.

(48) Tang, H.; Yan, F.; Lin, P.; Xu, J.; Chan, H. L. W. Highly Sensitive Glucose Biosensors Based on Organic Electrochemical Transistors Using Platinum Gate Electrodes Modified with Enzyme and Nanomaterials. *Adv. Funct. Mater.* **2011**, *21* (12), 2264–2272. https://doi.org/10.1002/adfm.201002117.

(49) Kergoat, L.; Piro, B.; Simon, D. T.; Pham, M. C.; Noël, V.; Berggren, M. Detection of Glutamate and Acetylcholine with Organic Electrochemical Transistors Based on Conducting Polymer/Platinum Nanoparticle Composites. *Adv. Mater.* **2014**, *26*, 5658–5664. https://doi.org/10.1002/adma.201401608.

(50) Khan, S.; Ali, S.; Khan, A.; Wang, B.; Bermak, A. Printing Sensors on Biocompatible Substrates for Selective Detection of Glucose. *IEEE Sens. J.* **2020**, *21* (4), 4167–4175. https://doi.org/10.1109/jsen.2020.3032539.

(51) McManus, D.; Vranic, S.; Withers, F.; Sanchez-Romaguera, V.; Macucci, M.; Yang, H.; Sorrentino, R.; Parvez, K.; Son, S. K.; Iannaccone, G.; Kostarelos, K.; Fiori, G.; Casiraghi, C. Water-Based and Biocompatible 2D Crystal Inks for All-Inkjet-Printed Heterostructures. *Nat. Nanotechnol.* **2017**, *12* (4), 343–350. https://doi.org/10.1038/nnano.2016.281.

(52) Parvez, K.; Worsley, R.; Alieva, A.; Felten, A.; Casiraghi, C. Water-Based and Inkjet Printable Inks Made by Electrochemically Exfoliated Graphene. *Carbon N. Y.* **2019**, *149*, 213–221. https://doi.org/10.1016/j.carbon.2019.04.047.

(53) Lingstedt, L. V; Ghittorelli, M.; Lu, H.; Koutsouras, D. A.; Marszalek, T.; Torricelli, F.; Cra, N. I.; Blom, P. W. M. Effect of DMSO Solvent Treatments on the Performance of PEDOT : PSS Based Organic Electrochemical Transistors. *Adv. Electron. Mater.* **2019**, *5*,

1–8. https://doi.org/10.1002/aelm.201800804.

(54) Fernandes, I. J.; Aroche, A. F.; Schuck, A.; Lamberty, P.; Peter, C. R.; Hasenkamp, W.; Rocha, T. L. A. C. Silver Nanoparticle Conductive Inks: Synthesis, Characterization, and Fabrication of Inkjet-Printed Flexible Electrodes. *Sci. Rep.* **2020**, *10* (8878), 1–11. https://doi.org/10.1038/s41598-020-65698-3.

(55) Bickerstaff, G.; Koudelka-Hep, M.; de Rooij, N. F.; Strike, D. J. Immobilization of Enzymes on Microelectrodes Using Chemical Crosslinking. In *Methods in biotechnology*; 1997; Vol. 1, pp 83–86. https://doi.org/10.1385/0-89603-386-4:83.

(56) Ji, X.; Lau, H. Y.; Ren, X.; Peng, B.; Zhai, P.; Feng, S.; Chan, P. K. L. Highly Sensitive Metabolite Biosensor Based on Organic Electrochemical Transistor Integrated with Microfl Uidic Channel and Poly (N-Vinyl-2-Pyrrolidone) -Capped Platinum Nanoparticles. *Adv. Mater. Technol. 2016,* **2016**, *1* (1600042), 1–8. https://doi.org/10.1002/admt.201600042.

(57) Keene, S. T.; Marais, A.; Curto, V. F.; Salleo, A.; Parlak, O. Molecularly Selective Nanoporous Membrane-Based Wearable Organic Electrochemical Device for Noninvasive Cortisol Sensing. *Sci. Adv.* **2018**, *4*, 1–10. https://doi.org/10.1126/sciadv.aar2904.

(58) Sensi, M.; Berto, M.; Candini, A.; Liscio, A.; Cossarizza, A.; Beni, V.; Biscarini, F.; Bortolotti, C. A. Modulating the Faradic Operation of All-Printed Organic Electrochemical Transistors by Facile in Situ Modification of the Gate Electrode. *ACS Omega* **2019**, *4* (April), 5374–5381. https://doi.org/10.1021/acsomega.8b03319.

(59) Khan, S.; Ali, S.; Khan, A.; Wang, B.; Bermak, A. Printing Sensors on Biocompatible Substrates for Selective Detection of Glucose. *IEEE Sens. J.* **2020**, No. c, 1–1. https://doi.org/10.1109/jsen.2020.3032539.

(60) Fiorito, P. A.; Córdoba De Torresi, S. I. Glucose Amperometric Biosensor Based on the Co-Immobilization of Glucose Oxidase (GOx) and Ferrocene in Poly(Pyrrole) Generated from Ethanol/Water Mixtures. *J. Braz. Chem. Soc.* **2001**, *12* (6), 729–733. https://doi.org/10.1590/S0103-50532001000600007.

(61) Yano, M.; Koike, K.; Mukai, K.; Onaka, T.; Hirofuji, Y.; Ogata, K. I.; Omatu, S.; Maemoto,

T.; Sasa, S. Zinc Oxide Ion-Sensitive Field-Effect Transistors and Biosensors. *Phys. Status Solidi Appl. Mater. Sci.* **2014**, *211* (9), 2098–2104. https://doi.org/10.1002/pssa.201300589.

(62) Zhen, X. V.; Rousseau, C. R.; Bühlmann, P. Redox Buffer Capacity of Ion-Selective Electrode Solid Contacts Doped with Organometallic Complexes. *Anal. Chem.* **2018**, *90* (18), 11000–11007. https://doi.org/10.1021/acs.analchem.8b02595.

(63) MacChia, E.; Picca, R. A.; Manoli, K.; Di Franco, C.; Blasi, D.; Sarcina, L.; Ditaranto, N.; Cioffi, N.; Österbacka, R.; Scamarcio, G.; Torricelli, F.; Torsi, L. About the Amplification Factors in Organic Bioelectronic Sensors. *Mater. Horizons* **2020**, *7* (4), 999–1013. https://doi.org/10.1039/c9mh01544b.

For Table of Contents Only